Progressive ladder network topology combining interferometric and intensity fiber-optic-based sensors

A. B. Lobo Ribeiro, R. F. Caleya, and J. L. Santos

Progressive ladder topology is studied by consideration of its properties of power budget and coupler tailoring. Optimization criteria are addressed for lossless and real systems, and their basic characteristics are compared with other topologies. Numerical results are presented, and an experiment is described for the case in which the network supports interferometric and intensity (with referentiation) fiber-optic-based sensors.

1. Introduction

Fiber-optic sensor technology has now reached a stage of development and maturity that fully justifies its application in many sensing problems.[1,2] Several light-encoding principles have been considered to detect the action of physical measurands, such as intensity, phase, polarization, and wavelength of the radiation. Considerable attention has been given to intensity- and phase-based (interferometric) sensors; the first are generally simple in design and inexpensive, and the second have the potential to provide extremely high sensitivities.[3]

In any case, for applications in which arrays of sensors are needed, the multiplexing of fiber-optic sensors will result in architectural simplicity and also in significant cost savings because of a reduction in the number of light sources, detectors, and fiber transmission lines required.[4,5] In general, multiplexing involves the concepts of network topology, sensor addressing, and sensor interrogation (i.e., demodulation).[6] These concepts are frequently not independent, which means that the choice of one implies the selection of the other two. Other features are also relevant, conditioning the possible configurations to solve a given problem. As an example, the integration in a network of interferometric and intensity-based sensors implies that it is in general problematic for the network to be reflective, as this is much more natural for the transmissive configurations (this is so because the intensity sensors are normally implemented in a multimode fiber, implying the need for the return fiber bus also to be multimode, which is feasible only if the network is transmissive). The sensor addressing can be in time, in frequency, in coherence, and in wavelength.[6] In connection with the recent development of intracore fiber grating devices, wavelength addressing is emerging as an extremely important phenomenon in a large range of applications.[7,8]

Figure 1 shows what can be considered to be the basic topologies for sensor networks.[5,9] Normally it is highly desirable that all sensors in a given network return the same level of average optical power (I_s) to the detection block. For some topologies, this is obtained without the necessity of imposing constraints on the power splitting ratio k of the couplers along the network, which is obviously a significant advantage because it permits all the couplers to be equal (to be rigorous, this is true only when the network losses are neglected). In addition, it is desirable that in a network of N sensors, I_s is large, the number of couplers is small, and intrinsic cross talk is not present (i.e., cross talk related to the structure of the sensing array). It must be pointed out that the addressing scheme can introduce extra cross talk between sensors. In consideration of these features, Table 1 compares the topologies shown in

A. B. Lobo Ribeiro and J. L. Santos are with the Grupo de Optoelectrónica, Instituto de Engenharia de Sistemas e Computadores, Rua Jose Falcão 110, 4000 Porto, Portugal. J. L. Santos is also with Laboratorio de Física, Universidade do Porto, Pr. Gomes Teixeira, 4000 Porto, Portugal. R. F. Caleya is with the Departamento Electrónica, Universidade do Alfonso X El Sáio, Avenida Universidad 1, 28691 Villanueva de la Cañada, Madrid, Spain.

Received 17 November 1994; revised manuscript received 27 February 1995.

0003-6935/95/286481-08$06.00/0.

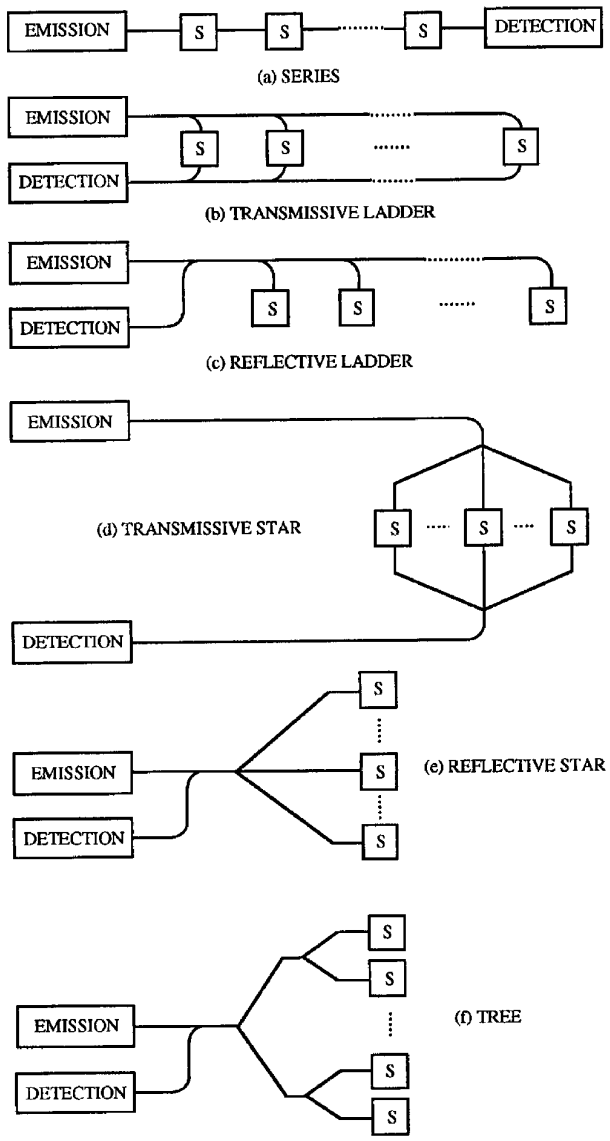

Fig. 1. Basic topologies of optical-fiber networks.

Fig. 1, where I_0 is the average optical power injected into the network (it is assumed that the network is lossless and that the sensors have unit transmissivity or reflectivity).

Table 1. Comparison of the Network Topologies Shown in Fig. 1

Topology	Number of Couplers	Equal Couplers	Optical Power per Sensor	Instrinsic Cross Talk
Series	0	—	I_0	Yes
Transmissive ladder	$2(N-1)$	No	I_0/N^2	No
Reflective ladder	N	No	$I_0/4N^2$ [a]	No
Transmissive star	2^b	Yes	I_0/N^2	No
Reflective star	2^c	—	$I_0/4N^2$	No
Tree[d]	N	Yes	$I_0/4N^2$	No

[a]For the first coupler it is assumed that $k_1 = 0.5$ (optimum case).
[b]These couplers are of the type $1 \rightarrow N$ $(k = 1/N)$.
[c]One coupler is a 2×2 and the other is a $1 \rightarrow N$.
[d]The optimum situation occurs for $N = 2^i$, $i = 1, 2, 3, \ldots$, and for $k = 0.5$.

Several other more exotic sensing topologies have been considered in the literature, e.g., the recursive series topology[10] and the tapped serial array.[11] However, in general these configurations are, to some extent, constrained by the level of intrinsic cross talk present. Figure 2(a) shows an interesting topology that, to our knowledge, has not been analyzed so far (it was briefly mentioned in Ref. 12 in the context of sensing applications for avionics). This is referred to as the progressive ladder topology (PLT) and is studied in detail here. For the purpose of comparison, Fig. 2(b) depicts the well-known transmissive ladder topology (TLT), which probably is the one that has been more utilized in sensing applications.

2. System Design

In Fig. 2 the optical-fiber sensors can be of any type; in particular, they can be interferometric or intensity-based sensors. For simplicity it is assumed that their transmissivity is unitary. Assume that there are N sensors in the ladder placed in the rungs that are numbered 1 through N, with a variable i beginning with $i = 1$ for the rung nearest to the light source. Let the magnitude of the amplitude coupling coefficient for the coupler associated with sensor i be $\sqrt{k_i}$ [with the exception of $k_1 = k_{\text{in}}$ and $k_N = k_{\text{out}}$ for Fig. 2(a)], so that a fractional power k_i is transferred between the two fibers in coupler i, and a power $(1 - k_i)$ passes straight through. The crucial criterion for system design is to ensure that each sensor returns the same average optical power (I_s) from each rung of the array to the detector, i.e., $I_s(i) = I_s(i + 1)$ for all i between 1 and $N - 1$.[13] Two cases are considered below.

A. Lossless System

Using the above criterion for the PLT network, we derive the relations between the coupling ratios:

$$k_i = k, \forall_N, \quad i = 2, \ldots, N-1,$$
$$k_{\text{in}} = k_{\text{out}} = k_0 = \frac{k^2}{k^2 - k + 1}. \tag{1}$$

Therefore, with the exception of the first and last couplers, which occupy an asymmetric location in the network, all other couplers have to have equal power-coupling ratios $(k_i = k)$. This property is highly de-

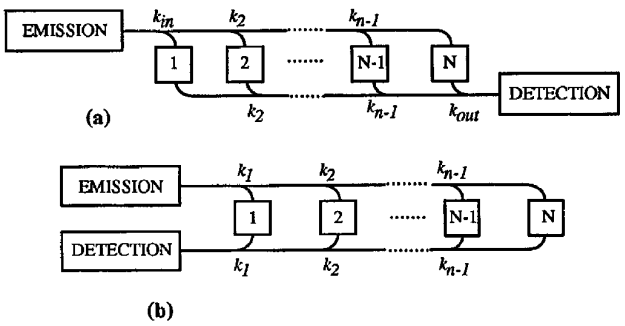

Fig. 2. Ladder topologies: (a) progressive, (b) transmissive.

sirable because it avoids the coupler tailoring along the network, which has implications in terms of system cost and, very importantly, facilities of maintenance and repair procedures. In Eq. (1) the freedom of choice of power-coupler ratios can be used with advantage to select the optimum coupling value ($k = k_{\mathrm{opt}}$) that maximizes the return average power per sensor (I_s). This value can be obtained when the derivative of the return power is set with respect to k, i.e., $\mathrm{d}I_s/\mathrm{d}k = 0$.[13] The result is

$$k^3(N-3) + k^2(3-N) + k(N+1) - 2 = 0. \tag{2}$$

The solution of this polynomial is given by

$$k = k_{\mathrm{opt}} = \frac{1}{3} - \frac{0.84(N+3)}{A\sqrt{N-3}} + \frac{0.26A}{\sqrt{N-3}},$$

$$A = [39\sqrt{N-3} - 7N\sqrt{N-3} + 3^{3/2}(3N^3 - 15N^2 + 149N - 137)^{1/2}]^{1/3}. \tag{3}$$

In contrast, for the TLT network the couplers have to be tailored through the relation

$$k_i = \frac{1}{N-i+1}, \quad i = 1, \ldots, N-1. \tag{4}$$

Figure 3(a) clearly illustrates this difference for the case $N = 10$; for the PLT case it is represented by $k = k_{\mathrm{opt}}$ in Eqs. (3). From these results, the return powers per sensor for the PLT and TLT configurations are given, respectively, by

$$I_{s(\max)}|_{\mathrm{PLT}} = I_0 k_0 (1-k_0)(1-k_{\mathrm{opt}})^{N-2}, \tag{5}$$

$$I_s|_{\mathrm{TLT}} = \frac{I_0}{N^2}. \tag{6}$$

Figure 3(b) shows, as a function of N, plots for $I_{s(\max)}|_{\mathrm{PLT}}$ and $I_s|_{\mathrm{TLT}}$. Interestingly, the two curves are similar, with the performance of the TLT being slightly better (e.g., for $N = 10$, $I_s|_{\mathrm{TLT}}$ is larger than $I_{s(\max)}|_{\mathrm{PLT}}$ by a factor of 1.3).

B. Real System

The analysis is simplified if it is assumed that losses in fibers, splices, couplers, and so on are lumped together in the couplers, giving a total power attenuation factor of $1-\beta$ and $1-\gamma$ each time the light crosses a coupler in the input and output buses, respectively. (We consider two different attenuation factors to include also the situation in which, to permit time addressing, we insert delay lines of length L between sensing branches in the input bus of the configuration shown in Fig. 2). Therefore, from Fig. 2 it can be seen that $1-\beta$ is approximately equal to the total loss in the coupler, in a length L of fiber and in two fusion splices; $1-\gamma$ is the lumped loss relative to one coupler and to one splice. The following set of equations emerges from the investigation of the PLT network (to get equal return power from all the sensors):

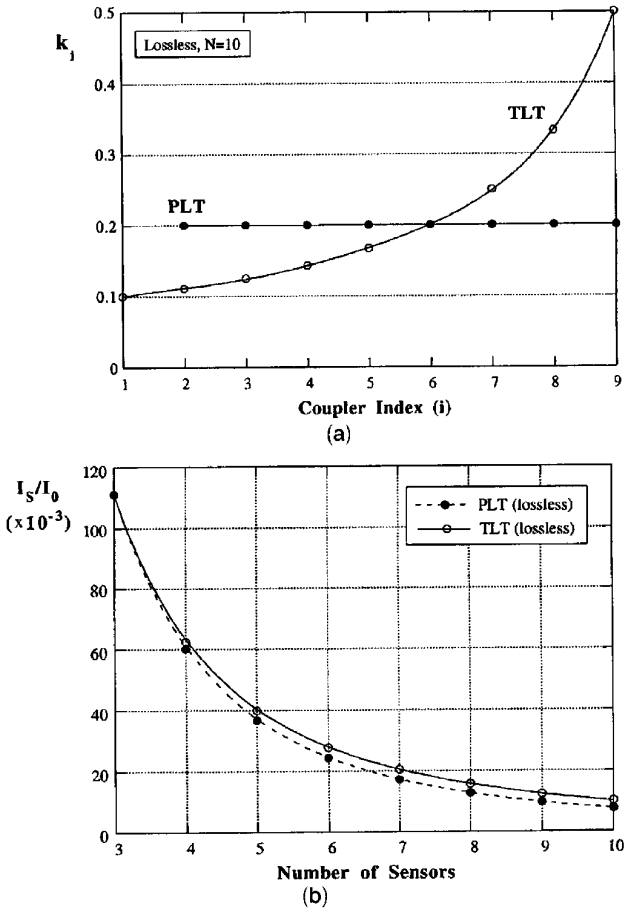

Fig. 3. (a) Power ratio of the couplers as a function of their locations in the array ($N = 10$) for the lossless system. For the PLT case the optimum value given by Eqs. (3) is shown [$N = 10$, $k_{\mathrm{in}}(\mathrm{opt}) = k_{\mathrm{out}} = 0.05$]. (b) Returned average power per sensor (normalized by the input power) for the progressive and transmissive ladder topologies.

$$k_{\mathrm{out}} = \left[\left(\frac{1-k_{\mathrm{in}}}{k_{\mathrm{in}}}\right)\left(\frac{\beta}{\gamma}\right)^{N-1} + 1\right]^{-1}, \tag{7a}$$

$$k_{N-1} = \frac{-\beta k_{\mathrm{out}} + [\beta^2 k_{\mathrm{out}}{}^2 + 4\gamma\beta k_{\mathrm{out}}(1-k_{\mathrm{out}})]^{1/2}}{2\gamma(1-k_{\mathrm{out}})}, \tag{7b}$$

$$k_i = \frac{-\beta k_{i+1}{}^2 + k_{i+1}[\beta^2 k_{i+1}{}^2 + 4\gamma\beta(1-k_{i+1})]^{1/2}}{2\gamma(1-k_{i+1})}, \quad i = 2, \ldots, N-2 \wedge N \geq 4. \tag{7c}$$

There is again freedom to choose k_{in}, which can be used to maximize the average return power from the sensors. It was not found trivial to obtain analytical solutions for $k_{\mathrm{in}} = k_{\mathrm{in}}(\mathrm{opt})$. However, it is relatively straightforward to get numerical results from Eqs. (7a)–(7c). Figure 4 shows $k_{\mathrm{in}}(\mathrm{opt})$ as a function of N for $\beta = 0.84$ and $\gamma = 0.93$, which means lumped losses of 0.75 dB and 0.3 dB, respectively [considering operation at 1300 nm, we obtained these values from

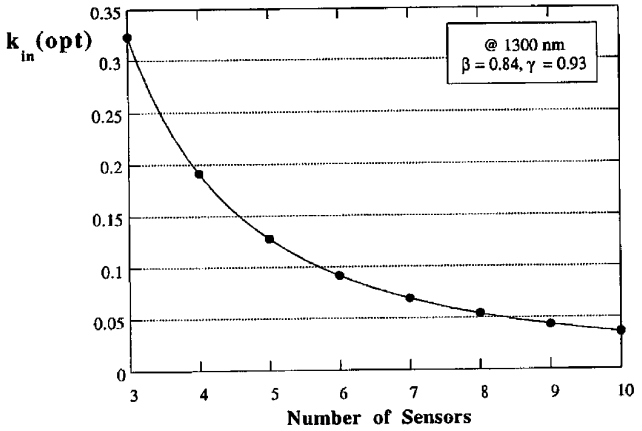

Fig. 4. $k_{\text{in}}(\text{opt})$ versus the number of sensors N for a real system ($\beta = 0.84$, $\gamma = 0.93$ at 1300 nm).

fiber loss ($L = 500$ m) = 0.25 dB, coupler loss = 0.1 dB, splice loss = 0.2 dB]. For the TLT case it is possible to find a closed form for k_i, namely,

$$k_i = \frac{(\beta\gamma)^{(N-i)/2}}{\sum_{m=i}^{N} (\beta\gamma)^{(N-m)/2}}, \qquad i = 1, \ldots, N-1. \tag{8}$$

For these two topologies, Fig. 5(a) shows k_i versus i for $N = 10$, $\beta = 0.84$, and $\gamma = 0.93$; for the PLT case it was considered $k_{\text{in}} = k_{\text{in}}(\text{opt})$, with the value extracted from Fig. 4. Comparing Figs. 3(a) and 5(a), we can observe that for the PLT the introduction of losses in the network implies that one can fulfill the condition of equal return power from all the sensors in the network only by addressing different values for the different k_i's through the array. However, not considering the special cases of k_{in} and k_{out}, we find it remarkable to observe that the spread of values is relatively small, in strong contrast with the TLT case. Therefore, the PLT is an intrinsically balanced configuration, which is a highly desirable characteristic because of the reasons already mentioned in the context of the analysis of the lossless system. Using Eqs. (7) and (8) we can calculate the return power per sensor for the PLT and TLT cases, respectively, as

$$I_{s(\max)}|_{\text{PLT}} = I_0 \gamma^{N-1} k_{\text{in}}(\text{opt})(1 - k_{\text{out}}) \prod_{i=2}^{N-1} (1 - k_i), \tag{9}$$

$$I_s|_{\text{TLT}} = I_0 \frac{(\beta\gamma)^{N-1}}{\left[\sum_{m=i}^{N} (\beta\gamma)^{(N-m)/2}\right]^2}. \tag{10}$$

In Eq. (9), k_{out} and k_i are given by Eqs. (7). Figure 5(b) shows, as a function of N, plots for $I_{s(\max)}|_{\text{PLT}}$ and $I_s|_{\text{TLT}}$. In line with the behavior observed in Figs. 3(b) and 5(b) and from the viewpoint of the sensor-returned average optical power, the configurations of PLT and TLT are very similar. An analysis of Table 1 shows that, not considering the singular case of the series topology, the TLT (together with the transmissive star topology) has the highest value for the return power per sensor. Therefore, the PLT is also favorable in terms of power budget, with the corresponding positive implications in terms of sensor sensitivity. In general, it is very convenient that the emitter and detector blocks be physically together, as elements of a single optoelectronic unit. The TLT network fulfills this condition but the PLT does not. However, this is not an essential limitation of this configuration because it is always possible, with negligible degradation in performance (and in cost), to guide the light that exists in the array to the detection and processing unit physically located in the input block.

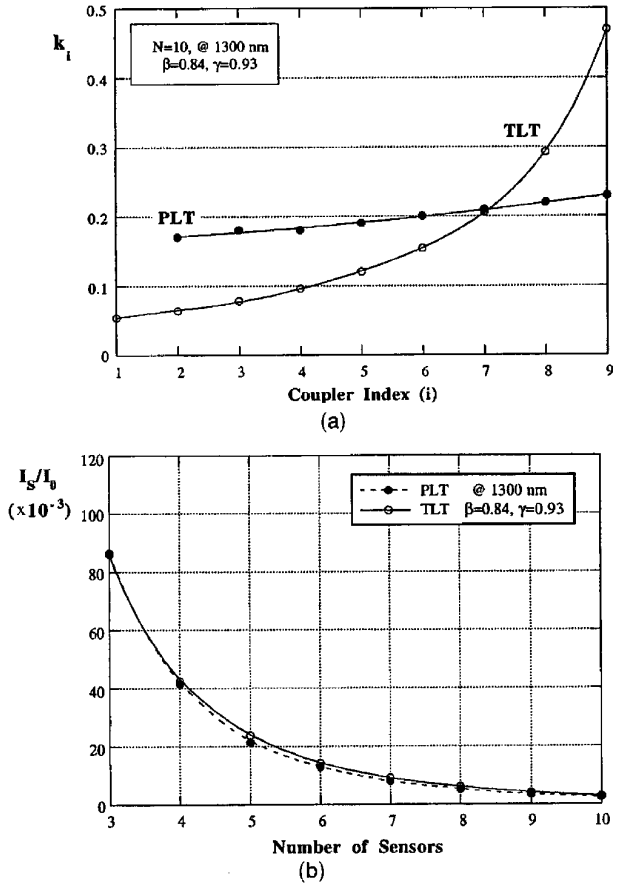

Fig. 5. (a) Power ratios of the couplers as a function of their locations in the array ($N = 10$, for the real system; $\beta = 0.84$, $\gamma = 0.93$ at 1300 nm). For the PLT the optimum values are presented. (b) Returned average power per sensor (normalized by the input power; $\beta = 0.84$, $\gamma = 0.93$ at 1300 nm).

If the sensors are addressed in time, it is necessary to ensure that the return signals from different sensors have allocated different time slots. Therefore, if a rectangular optical waveform is injected into the input fiber with a period T and pulse duration μ, then the following conditions must be satisfied:

$$\frac{nL}{c} \geq \mu,$$

$$T \geq \frac{(N-1)nL}{c} + \mu, \tag{11}$$

where n is the refractive index of the fiber-guided mode and L is the length of the fiber delay lines inserted between the sensing branches of the networks. If the equalities in conditions (11) are considered and if I_{peak} is the peak power injected into the input fiber, then the injected average power I_0 is

$$I_0 = \frac{\mu}{T} I_{\text{peak}} = \frac{I_{\text{peak}}}{N}. \tag{12}$$

In addition, with time-division multiplexing, each sensor in the array is sampled in time; therefore, the complete recovery of the information sent by the sensors requires that the sampling period, T, satisfy the condition (Nyquist's criteria)

$$T \leq \frac{1}{2f_{\max}}, \tag{13}$$

where $f_{\max}$ is the spectral component of highest frequency present in the signals arriving at the sensors.

3. Experiment

The PLT described above was tested for three sensors ($N = 3$); the first two were Mach–Zehnder interferometers and the third was an intensity-based curvature sensor. Figure 6 shows the experimental arrangement. The last section of the ladder, which supports the intensity sensor and the corresponding referentiation structure, was implemented by the use of multimode fiber and couplers (graded-index fiber, 50/125 μm). Because of the practical impossibility of the realization of fabricated tailored couplers, i.e., k_{in} and k_{out}, to optimize the returned power (I_s) of the sensors, all couplers in the network had a nominal splitting ratio of ≈50/50. Addressing the sensors was, in time, through pulse modulation of the light injected into the network in combination with the fiber delay lines, L_1 and L_2. A fraction of the light pulse to the intensity sensor is directed to a reference arm, which is separated in time from the sensing pulse through the insertion of fiber delay line L_3. The length of these delay lines was ≈500 m.

The optical source used was a laser diode (Melles–Griot 06DLS407, $\lambda = 785$ nm, temperature controlled) operating 28 mA above threshold and emitting ≈20 mW of optical power in a single longitudinal mode. A Faraday isolator (insertion loss of 0.77 dB) was used to avoid the reinjection of backreflected radiation into the laser cavity. Pulse modulation of the optical power injected into the network was achieved by the use of an acousto-optic modulator (AOM, Newport N23080), driven by a square waveform (frequency of 83 kHz, duty cycle of ≈20%). The average optical power injected into the fiber was ≈300 μW, corresponding to an emitted power of ≈2 mW from the first diffraction order of the AOM. This low optical power value is due to the poor efficiency of the AOM, which was not specified for this operating wavelength. The optical signal output was detected by a hybrid photodetector plus amplifier (from UOL, Ltd., RM800) with an effective responsivity and an NEP of 0.37 V/μW and 0.33 pW/$\sqrt{\text{Hz}}$, respectively. After amplification the electrical signal was applied to the electronic time demultiplexer based on an asynchronous scheme (which will be described elsewhere), not requiring direct synchronization from the AOM modulating electronics.

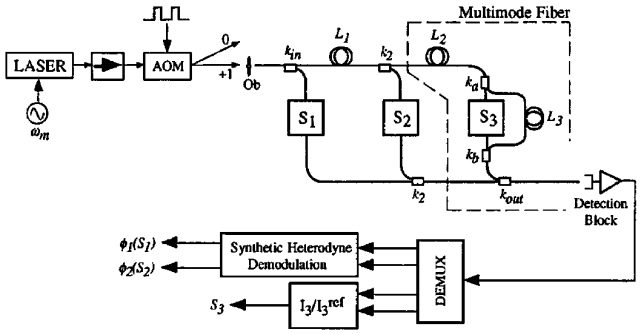

Fig. 6. Experimental arrangement (the nominal power ratio of all couplers is 0.5).

To apply test signals, we incorporated piezoelectric transducers (PZT's) in one of the arms of each Mach–Zehnder interferometer (i.e., sensors 1 and 2), which had efficiencies of 0.37 rad/V and 0.32 rad/V, respectively. We performed the demodulation of these interferometric signals by using the synthetic heterodyne technique,[14] which required a sinusoidal modulation (ω_m) of the laser diode current (to get a corresponding frequency modulation of the light emitted; for this laser, $\delta v/\delta i = 5.4$ GHz/mA), together with a certain path-length imbalance of the interferometers ($\Delta L \approx 3.8$ cm). Modulation of the laser frequency by application of a sinusoidal waveform, $\Delta i_m \sin(\omega_m t)$, to the injection current of the laser diode gives rise to an interferometric phase modulation, $\Delta\phi$, at the output of an unbalanced interferometer, which is given by

$$\Delta\phi = \frac{2\pi n \Delta L}{c} \Delta i_m \left(\frac{\delta v}{\delta i}\right) \sin(\omega_m t) = \Delta\phi_m \sin(\omega_m t), \tag{14}$$

where n is the effective mode refractive index and c is the free-space velocity of light.

Standard theoretical analysis indicates that, if the laser amplitude modulation (Δi_m) is adjusted such that $\Delta\phi_m = 2.63$ rad, i.e., $J_1(\Delta\phi_m) = J_2(\Delta\phi_m)$, where $J_a(\Delta\phi_m)$ with $a = 0, 1, 2, \ldots$ are the first-order Bessel functions, at the output of the synthetic heterodyne electronic system we obtain[14]

$$S_0 = a I_s \vartheta J_1(\Delta\phi_m) \cos[\omega_c t + \phi_s(t)], \tag{15}$$

where I_s is the return average optical power from the sensor, ϑ is the fringe visibility, a is a constant factor taking into account the losses in the detection system, ω_c is an electronic generated frequency carrier, and $\phi_s(t)$ is the output phase of the interferometric sensor, which contains the signal phase information of interest. Thus it is straightforward to recover the phase information from this heterodyne carrier signal [Eq.

(15)] by the use of frequency discrimination or a phase-locked loop with subsequent integration. The amplitude modulation used was 0.42 mA (at 24 kHz), the value required to obtain the optimum synthetic heterodyne demodulation condition, i.e., $J_1 = J_2$.[14] For the intensity sensor (sensor 3), demodulation simply consisted of the ratio between the signal and reference pulses, which eliminates all the power fluctuations that can arise along the system (laser power fluctuations, injection conditions, losses in the input and return buses, etc.).

4. Results and Discussion

Figure 7(a) shows the pulse train at the detector output (for a better view of the input waveforms, the duty cycle was reduced to a value smaller than 20%). The first three pulses are relative to the sensors and the fourth is the reference pulse of the intensity sensor (a large phase signal was applied to the PZT's in the sensing interferometers, permitting the determination of the interferometric fringe visibility, i.e., ≈70%). The amplitudes of the pulses shown in this figure can be understood in terms of the analysis presented in Section 2, which yields

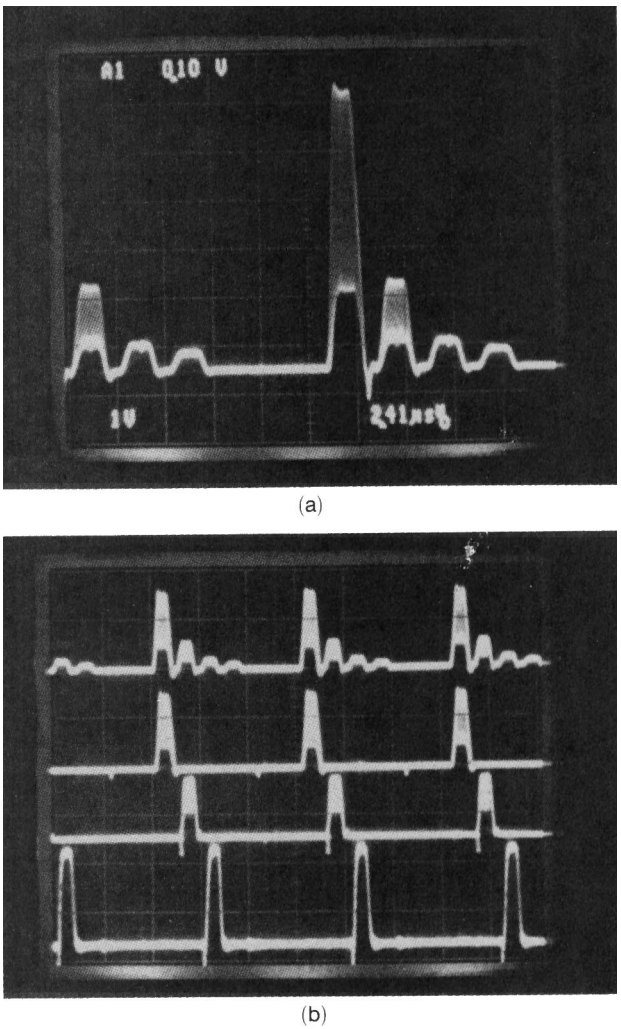

(a)

(b)

Fig. 7. (a) Detected signals at the output of the fiber network (1 V/div, 2.41 μs/div). (b) Input pulse train to the DEMUX (top) and the first three demultiplexed output signals, corresponding to sensors 1, 2 and 3.

$$I_1 = \frac{\alpha_1\gamma_1\gamma_2}{2^3} I_0,$$

$$I_2 = \frac{\alpha_2\beta\gamma_2}{2^4} I_0,$$

$$I_3 = \frac{\alpha_3\beta^2}{2^5} I_0,$$

$$I_3^{\text{ref}} = \frac{\alpha_4\beta^2}{2^5} I_0. \tag{16}$$

It is now necessary to consider two different γ parameters (γ_1 and γ_2), where $1 - \gamma_1$ is the lumped loss relative to a single-mode coupler and one single-mode splice and $1 - \gamma_2$ is the corresponding parameter relative to a single-mode–multimode splice and one multimode coupler. Here α_1 and α_2 are the transmissivities of sensors 1 and 2, considering their intrinsic values (0.5 for Mach–Zehnder interferometers) and the losses in the associated couplers and splices. Here α_3 is the transmissivity of the intensity sensor at the minimum power loss state, i.e., considering only the lumped loss relative to propagation through two multimode couplers and two splices. In turn, α_4 is the corresponding parameter for the referencing arm of the intensity sensor, i.e., $1 - \alpha_4$ is the lumped loss relative to propagation through two multimode couplers, three splices, and fiber delay line L_3. The parameter β was defined in Section 2.

The following values have been assumed: splice loss, 0.2 dB; loss in a single-mode coupler, 0.2 dB; loss in a multimode coupler, 0.5 dB; and loss in the delay lines (500 m), 1.9 dB (3.8 dB/km at 780 nm). Therefore, for the several parameters it turns out that $\beta = 0.57$, $\gamma_1 = 0.91$, $\gamma_2 = 0.85$, $\alpha_1 = \alpha_2 = 0.42$, $\alpha_3 = 0.72$, and $\alpha_4 = 0.45$. If the injected optical power (I_0) into the network is 300 μW, then from Eq. (16) the optical returned power of each pulse at the output will be $I_1 = 12.2$ μW, $I_2 = 3.8$ μW, $I_3 = 2.2$ μW, and $I_3^{\text{ref}} = 1.4$ μW. Comparing these theoretical results with the values extracted from Fig. 7(a), which gives $I_1 = 15.1$ μW, $I_2 = 4.3$ μW, $I_3 = 2.2$ μW, and $I_3^{\text{ref}} = 1.4$ μW, we obviously find a fairly good agreement. Figure 7(b) illustrates the operation of the asynchronous time demultiplexer (DEMUX), showing the input wave train and the signals at the first three DEMUX output channels. It is clear that the proper operation of this device, which does not require any synchronization with the AOM, is also insensitive to the problems related to the time delays along the system, which in synchronous DEMUX's implies the need for fine tuning between signals in the emission and detection electronics (if this is not the case, large levels of electronic cross talk will appear).

Figures 8(a) and 8(b) show the synthetic heterodyne demodulated output spectra of channels 1 and 2 (relative to sensors 1 and 2, respectively), when

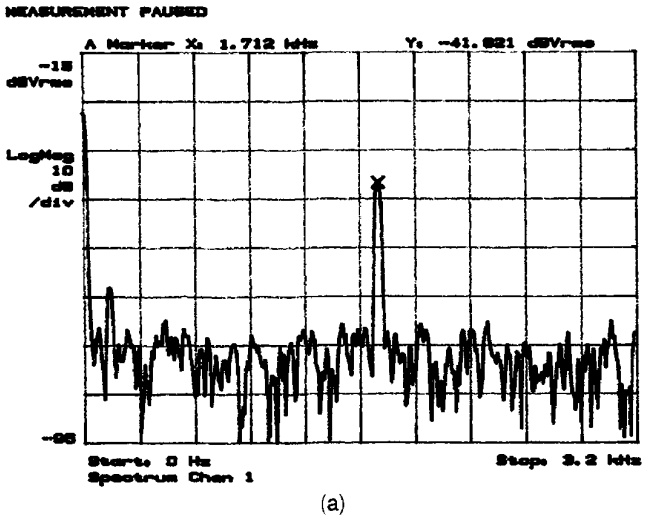

Fig. 8. Demodulated-output-spectra signals of sensors 1 and 2 when the PZT's are driven by sinusoidal-phase test signals of (a) an amplitude of 118 mrad and a frequency of 1.7 kHz (sensor 1), and (b) an amplitude of 102 mrad and a frequency of 2.6 kHz (sensor 2).

sinusoidal test signals with an amplitude of 0.32 V at frequencies of 1.7 kHz (sensor 1) and 2.6 kHz (sensor 2) were applied to the PZT's in the interferometers. From these figures, signal-to-noise ratios of 39 and 33.4 dB, in a 32-Hz bandwidth, are obtained for channels 1 and 2, respectively. Taking into account the applied voltage and the PZT efficiencies (sensor 1 is 0.37 rad/V, sensor 2 is 0.32 rad/V), we find that the corresponding sensitivities are 234 and 386 $\mu\text{rad}/\sqrt{\text{Hz}}$. These values are relatively modest because of the large level of electronic noise generated in the asynchronous DEMUX, which is still in a developmental state (proper optimization would substantially reduce these values). Considering that electronic noise is dominant and the return power from sensor 2 is smaller than the return power from sensor 1 by a factor of 3.5, we see that this explains the worst value for the sensitivity of sensor 2.

In addition, we can see from these results that the cross-talk level between channels 1 and 2 is below the noise floor, which indicates proper operation of the electronic time DEMUX [also evident from Fig. 7(b)]. Figure 9 shows the ratio between the amplitudes of the third (I_3) and fourth (I_3^{ref}) pulses as a function of the normalized curvature radius of the fiber in the intensity sensor. It should be mentioned that, by using a mode scrambler, we obtained an approximate uniform power modal distribution in the input multimode fiber to the intensity sensor, which is essential considering that the light exiting the single-mode fiber will excite only the lower-order mode(s) of the multimode fiber. Two sets of data are presented, i.e., the laser working with injection currents of 46 mA and 51 mA, which corresponds to an emitted laser power of 3 mW and 6 mW, respectively. As we can see, ratio I_3/I_3^{ref} (performed electronically by integrated circuit AD534) is nearly equal for the two cases, illustrating the effectiveness of the referencing technique (it should be emphasized that any kind of intensity sensor could be considered in this experiment).

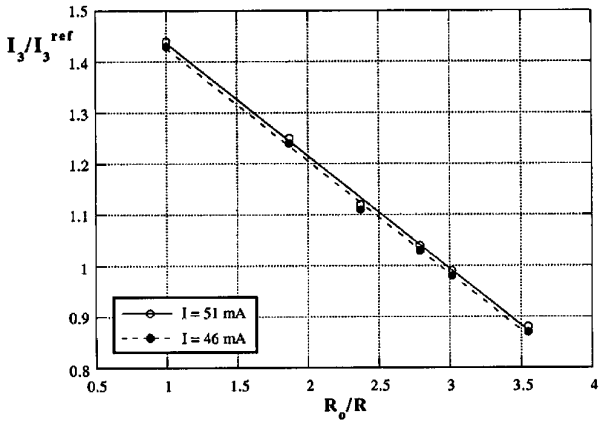

Fig. 9. Ratio between the sensing and referencing pulses of sensor 3 as a function of the fiber curvature radius of the sensing fiber (initial radius $R_0 = 6$ mm).

The network structure shown in Fig. 6 has the multimode section in the last rung of the ladder (clearly, it is the only acceptable light propagation from a single-mode to a multimode fiber). However, this is not a basic limitation, because if the return bus is implemented with the multimode fiber, then the intensity (made from multimode fiber) and the interferometric sensors can be placed in any order in the array. In conclusion, in this paper we have studied the progressive ladder topology, considering its properties in terms of network power budget and coupler tailoring. The problem of network optimization was addressed for both lossless and real systems, and their basic characteristics were compared with other topologies, namely the well-known transmissive ladder topology. We also emphasized the intrinsically balanced nature of the progressive array. The network concept was demonstrated with three sensors multiplexed in time; two of these were interferometric (Mach–Zehnders) and the other was an intensity-based sensor with referentiation.

A. B. Lobo Ribeiro acknowledges financial support from Programa PRAXIS XXI. R. F. Caleya acknowledges J. A. Martin Pereda and M. López-Amo and financial support from the Spanish Comisión Interministerial de Ciencia y Tecnología (TIC Program). Part of this research was performed in the framework of the Basic Research in Industrial Technologies–European Research on Advanced Materials NOSOST project.

References

1. E. Udd, *Fiber Optic Sensors,* 1st ed. (Wiley, New York, 1991), Chap. 1, p. 1.
2. G. Cancelliery, *Single-Mode Optical Fiber Measurement: Characterization and Sensing* (Artech, New York, 1993), Chap. 5, p. 271.
3. D. A. Jackson and J. D. C. Jones, "Optical fibre sensors," Opt. Acta **33,** 1469–1503 (1986).
4. J. P. Dakin, "Multiplexed and distributed optical fiber sensors," J. Phys. E **20,** 954–967 (1987).
5. D. A. Jackson, "Selected multiplexing schemes for fibre optic interferometric sensors," in *Distributed and Multiplexed Fiber Optic Sensors III,* J. P. Dakin and A. D. Kersey, eds., Proc. Soc. Photo-Opt. Instrum. Eng. **2071,** 68–72 (1993).
6. B. Culshaw and J. P. Dakin, *Optical Fiber Sensors: Systems and Applications* (Artech, London, 1989), Vol. 2, p. 511.
7. W. Morey, J. Dunphy, and G. Meltz, "Multiplexing fiber Bragg grating sensors," in *Distributed and Multiplexed Fiber Optic Sensors,* J. P. Dakin and A. D. Kersey, eds., Proc. Soc. Photo-Opt. Instrum. Eng. **1586,** 216–220 (1991).
8. A. D. Kersey, "Multiplexing fiber optic sensors," in *Distributed and Multiplexed Fiber Optic Sensors II,* J. P. Dakin and A. D. Kersey, eds., Proc. Soc. Photo-Opt. Instrum. Eng. **1797,** 161–187 (1992).
9. D. A. Jackson, A. B. Lobo Ribeiro, L. Reekie, and J. L. Archambault, "Simple multiplexing scheme for fiber optic grating sensor network," Opt. Lett. **18,** 1192–1194 (1993).
10. B. Moslehi, M. R. Layton, and H. J. Shaw, "Efficient fiber-optic structure with applications to sensor arrays," J. Lightwave Technol. **7,** 236–243 (1989).
11. A. D. Kersey and A. Dandridge, "Transmissive serial interferometric fiber sensor array," J. Lightwave Technol. **7,** 846–854 (1989).
12. R. M. Taylor and M. J. Ranshaw, "Coherence multiplexing polarimetric fiber sensor arrays for aerospace applications," Opt. Lasers Eng. **16,** 223–236 (1992).
13. J. L. Brooks, B. Moslehi, B. Y. Kim, and H. J. Shaw, "Time-domain addressing of remote fiber-optic interferometric sensor arrays," J. Lightwave Technol. **LT-5,** 1014–1023 (1987).
14. J. H. Cole, B. A. Danver, and J. A. Bucaro, "Synthetic-heterodyne interferometric demodulation," IEEE J. Quantum Electron. **QE-18,** 694–697 (1982).